Chemical Science

ROYAL SOCIETY OF CHEMISTRY

EDGE ARTICLE

View Article Online
View Journal | View Issue

Check for updates

Cite this: *Chem. Sci.*, 2024, **15**, 10830

All publication charges for this article have been paid for by the Royal Society of Chemistry

Received 23rd February 2024
Accepted 29th May 2024

DOI: 10.1039/d4sc01289e

rsc.li/chemical-science

Open Access Article. Published on 07 June 2024. Downloaded on 2/25/2026 12:12:19 AM. This article is licensed under a Creative Commons Attribution-NonCommercial 3.0 Unported Licence.

Flexible porous organic polymers constructed using C(sp^3)–C(sp^3) coupling reactions and their high methane-storage capacity†

Shuang Zhou,[a] Tianyu Qiu,[a] He Wang,[a] Boyan Tang,[a] Yang Su,[a] Tianhao Nan,[b] Junchao Dong,[a] Zihao Wang,[a] Dongtao Liu *[a] and Guangshan Zhu *[a]

Carbon–carbon coupling is a basic design principle for the synthesis of porous organic polymers, which are widely used in gas adsorption/separation, photocatalysis, energy storage, *etc.* However, the C(sp^3)–C(sp^3) coupling reaction to construct porous organic polymers remains an important yet elusive objective due to its low reactivity and unknown side reactions. Herein, we report that nickel bis(1,5-cyclooctadiene) ($Ni(COD)_2$), which was a famous catalyst for C(sp^2)–C(sp^2) coupling reactions, enables highly efficient C(sp^3)–C(sp^3) homo-coupling reactions to construct porous linear crystalline polymers and flexible three-dimensional porous aromatic frameworks (PAFs) under mild reaction conditions. The resulting linear polymers generated with dibromomethyl arenes have good crystallinity and high melting points (T_m = 286 °C) due to controllability of reaction sites. Furthermore, the PAFs (PAF-64, PAF-65 and PAF-66) stemmed from tri-/tetra-bromomethyl arenes show high surface area (S_{BET} = 390 m^2 g^{-1}) and high methane-storage capacity (up to 313 cm^3 cm^{-3}) because of their flexible frameworks. This work sheds new light on the construction of novel porous polymers through C(sp^3)–C(sp^3) coupling reactions and the development of methane-storage materials.

Introduction

Over the past few decades, multitudinous porous organic polymers (POPs) have been developed through transition-metal catalyzed carbon–carbon coupling reactions of C(sp^2) or C(sp). POPs always possess rigid structures, high surface area and excellent stability and can be widely applied in various fields including molecule adsorption/separation, photo/electro catalysis, energy storage, and environmental remediation.[1] For instance, porous aromatic frameworks (PAF-1) synthesized by C(sp^2)–C(sp^2) coupling polymerization exhibited exceptionally high surface area and outstanding gas storage.[2] Subsequently, the prevailing covalent C(sp)–C(sp) bond connecting the whole framework leads to a porous polymer network (PPN-1) with high thermal and chemical stabilities.[3] And then some porous polymers constructed by using C(sp^2)–C(sp) cross-coupling have also been reported, such as CMPs, PAF-26, PAF-28.[4–6] However, C(sp^3)–C(sp^3) coupling to construct POPs has not yet been reported,[7] although the Tan group reported a group of hyper-cross-linked microporous polymers (HCPs) that prepared by Friedel–Crafts reactions of arenes with dihaloalkanes (constructed using C(sp^3)–C(sp^2) bonds).[8] Note that the Wurtz reaction and Grignard coupling using transition-metal systems have been applied to catalyzed C(sp^3)–C(sp^3) coupling reactions.[9–11] However, they are often limited to small molecule reactions due to their harsh reaction conditions or low activity or inevitable side reactions.[7,12] Although some C(sp^3)–C(sp^3) coupling reactions also worked in the presence of transition-metal catalysts (Ni, Co, Cu, and Fe) and a suitable metallic reductant (Zn and Sm), very few direct coupling polymerizations have been implemented owing to the lower reactivity of C(sp^3).[13] To date, the low reactivity of C(sp^3) remains a big barrier that prevented the area of C(sp^3)–C(sp^3) coupling polymerization from blossoming.

On the other hand, natural gas, comprising primarily methane, has been considered a "clean fuel" to promote global environmental sustainability away from petroleum-based fuels to a green, low-carbon energy future. Compared with the traditional strategy of liquefied or compressed natural-gas storage, an adsorbed natural gas (ANG) storage system is a promising technology that uses nanoporous materials as adsorbents.[14–17] To date, numerous efforts have been made by designing new porous materials with ultrahigh porosity (such as MOFs) or pressure-triggered flexible frameworks,[18–22] but mostly fall short of the US Department of Energy targets for methane (0.5 g g^{-1}, 263 cm^3 cm^{-3}).[23–25] Moreover, natural gas

[a]*Department of Chemistry, Northeast Normal University, Changchun, Jilin 130024, P. R. China. E-mail: liudt737@nenu.edu.cn; zhugs100@nenu.edu.cn*

[b]*State Key Laboratory of Polymer Physics and Chemistry, Changchun Institute of Applied Chemistry, Chinese Academy of Sciences, Changchun, 130022, P. R. China*

† Electronic supplementary information (ESI) available. CCDC 2300607. For ESI and crystallographic data in CIF or other electronic format see DOI: https://doi.org/10.1039/d4sc01289e

© 2024 The Author(s). Published by the Royal Society of Chemistry

Open Access Article. Published on 07 June 2024. Downloaded on 2/25/2026 12:12:19 AM. This article is licensed under a Creative Commons Attribution-NonCommercial 3.0 Unported Licence.

inevitably contains small amounts of H_2O, H_2S, CO_2, and other impurities, which can attack ANG adsorbents and affect methane storage. Despite several recent achievements,[18–26] development of novel porous polymers with both high methane-storage capacity and excellent structural stability for ANG technology is still of great importance.

In this paper, a highly efficient C(sp^3)–C(sp^3) coupling polymerization catalyzed by Ni(COD)$_2$ was developed. When dibromomethyl arenes were used as monomers, porous linear polymers could be synthesized, and they showed good crystallinity and high melting points. With a switch to the monomers of tri-/tetra-bromomethyl aromatics, flexible PAFs with high surface area and good resistance to acids/alkalis were achieved. Moreover, these flexible frameworks exhibited a high volumetric working capacity (5–100 bar) of 313 cm^3 cm^{-3} for methane, which is 19% higher than the US DOE target (263 cm^3 cm^{-3}).

Results and discussion

The homocoupling of 4-bromomethylbiphenyl was used first as the model reaction for the study of the feasibility and location of the C(sp^3)–C(sp^3) coupling reaction (Fig. 1a). By using the Ni(COD)$_2$ system, a high conversion of 98% was achieved within 5 h, which is much higher than that by the $NiCl_2$ system and CuI system (Fig. 1b). ^{1}H and ^{13}C NMR spectra of the obtained 1,2-bis(diphenyl) ethane confirmed that the reaction successfully occurred (Fig. 1d). The single crystal structure of 1,2-bis(diphenyl) ethane (CCDC: 2300607) further proved that the carbon–carbon coupling reaction takes place precisely at the C–Br bond instead of random reaction sites (C–Br bond and C–H bond on the aromatic ring) in the Friedel–Crafts reaction (Fig. 1c).[25–28] We assess the current state of the art and summarize key transition-metal catalyst mechanistic studies.[9–11,29,30] In general, the reaction involves two steps: metallic reductants (generate reducing agents from metal halides) and organometallic nucleophiles (perform coupling). Although the reductant triggers the slow formation of organometallic nucleophiles, the "indirect" delivery offers a low and constant concentration of the nucleophilic species that couldn't afford enormous coupling polymerization conditions. Meanwhile, the less electrophilic [Ni]^0 catalyst, Ni(COD)$_2$, which served as a catalyst with bromomethyl aromatics for the C(sp^3)–C(sp^3) coupling reaction, directly triggers the formation of organometallic nucleophiles instead of an excess of metallic reductants (such as Sm, Mg, and Zn) to generate reducing agents. Finally, an efficient and fast catalytic system was developed to achieve the C(sp^3)–C(sp^3) coupling polymerization (Scheme 1).

Inspired by the above results, we tried the C(sp^3)–C(sp^3) coupling polymerization of dibromomethyl arenes, such as 1,2-bis(bromomethyl) benzene, 1,3-bis(bromomethyl) benzene, 1,4-bis(bromomethyl) benzene and 4,4′-bis(bromomethyl) biphenyl. To our delight, all polymerizations proceeded

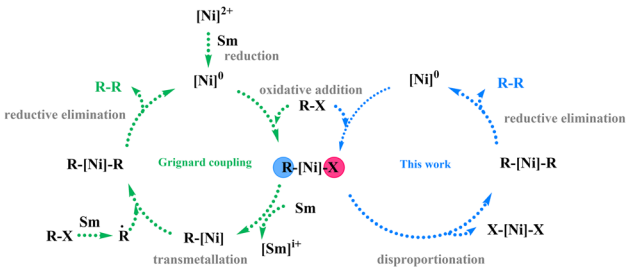

Scheme 1 The proposed carbon–carbon coupling mechanisms using the $NiCl_2$ or Ni(COD)$_2$ system.

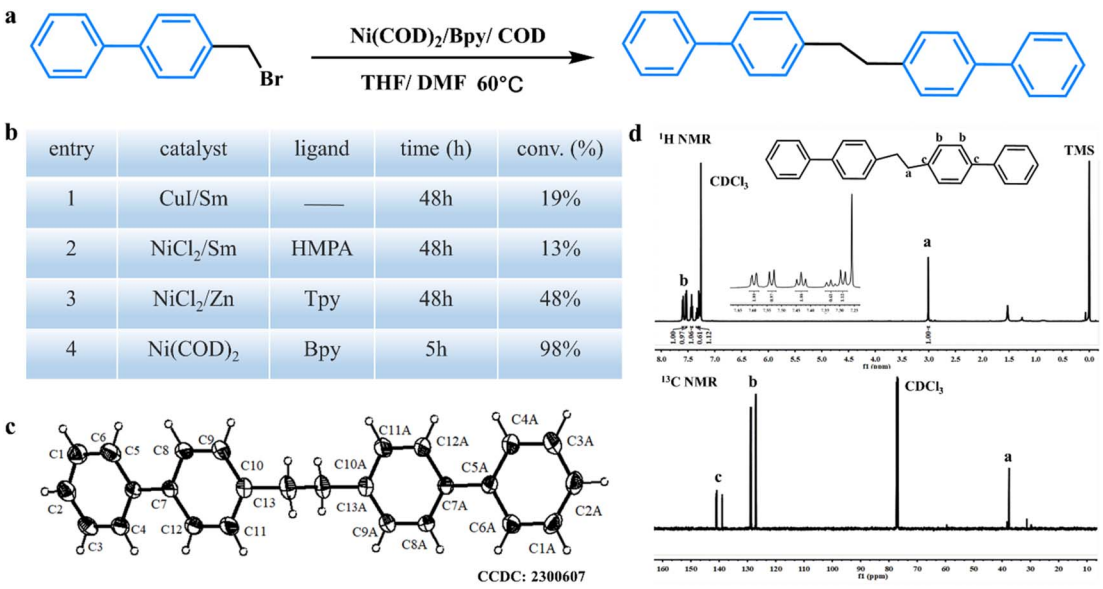

Fig. 1 Small molecule model reaction. (a) Synthesis of 1,2-bis(diphenyl) ethane. (b) Comparisons for the preparation of 1,2-bis(diphenyl) ethane with different catalytic systems. (c) X-ray single crystal structure of 1,2-bis(diphenyl) ethane. (d) ^{1}H NMR spectrum (above) and ^{13}C NMR spectrum (below) of 1,2-bis(diphenyl) ethane ($CDCl_3$, 25 °C).

Open Access Article. Published on 07 June 2024. Downloaded on 2/25/2026 12:12:19 AM.
This article is licensed under a Creative Commons Attribution-NonCommercial 3.0 Unported Licence.

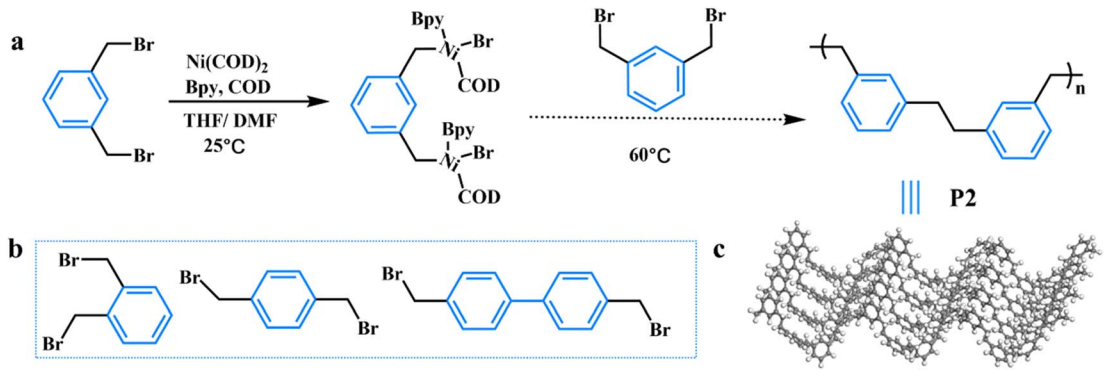

Fig. 2 Synthesis of linear polymers. (a) The synthetic route of P2 to produce the linear structure. (b) Monomer structures of P1, P3, and P4. (c) The molecular packing model of P2.

smoothly with high conversion. Four new linear polymers, including poly(1,2-bis(bromomethyl) benzene) (P1), poly(1,3-bis(bromomethyl) benzene) (P2), poly(1,4-bis(bromomethyl) benzene) (P3) and poly(4,4′-bis(bromomethyl) biphenyl) (P4), were achieved, as shown in Fig. 2. It should be noted that the obtained polymers can be considered linearly alternating copolymers of ethylene and benzene/biphenyl, which have hardly been synthesized by traditional polymerization methods. The structures of these polymers were well characterized using the corresponding ^{1}H NMR spectra and FTIR spectra, which demonstrated that all C–Br bonds converted to C–C bonds (Fig. S1–S4† and 3h). Owing to the introduction of a phenyl group in the main chain, these linear polymers exhibited excellent thermal stability by thermogravimetric analysis under N_2 ($T_{d,10\%\ loss}$ > 420 °C) (Fig. S5†). Scanning electron microscopy (SEM) and transmission electron microscopy (TEM) images showed that P1 and P2 presented layer structures while the morphology of P3 and P4 switched to particles (Fig. S6–S9†).

Moreover, these linear polymers possessed good crystallinity which was verified by powder X-ray diffraction (PXRD)

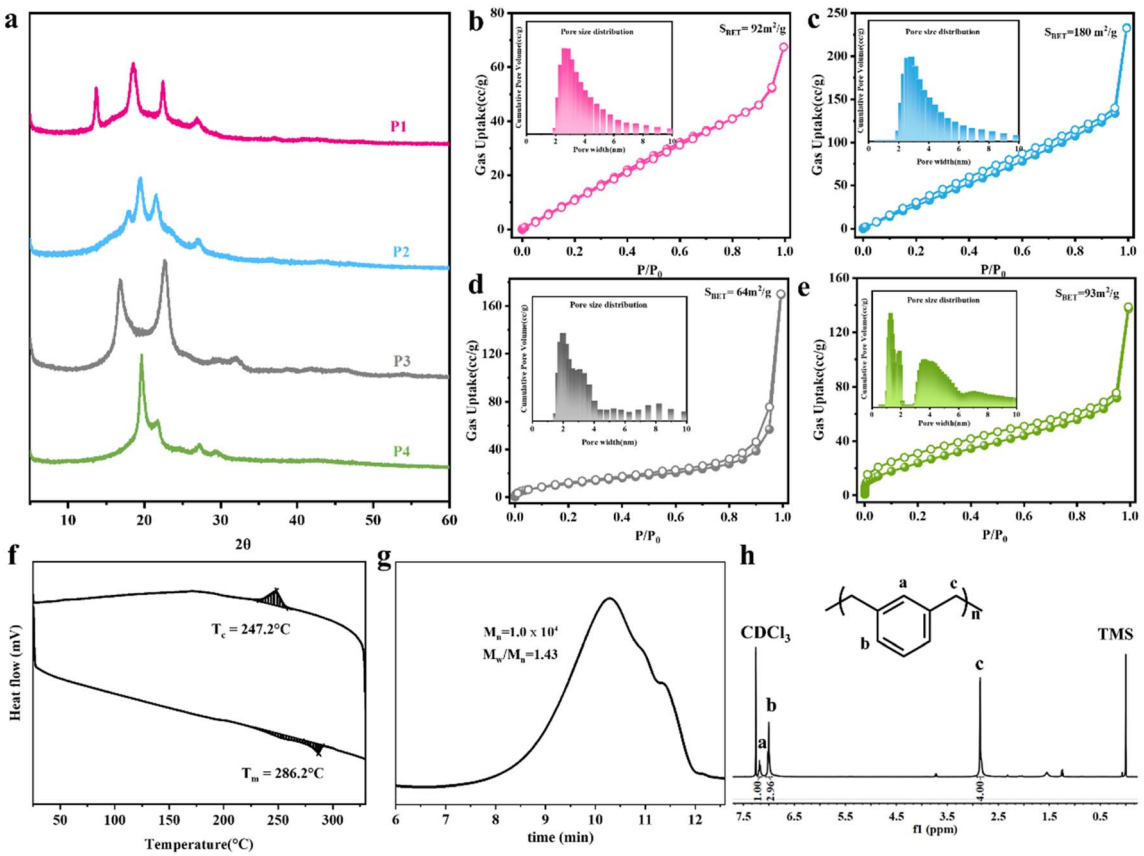

Fig. 3 (a) XRD patterns of the linear polymers. (b–e) N_2 adsorption–desorption isotherms and corresponding pore size distributions measured at 77 K for P1 (b), P2 (c), P3 (d) and P4 (e). (f) DSC curve of P3. (g) GPC curve of P2. (h) ^{1}H NMR spectrum of P2 ($CDCl_3$, 25 °C).

© 2024 The Author(s). Published by the Royal Society of Chemistry

Open Access Article. Published on 07 June 2024. Downloaded on 2/25/2026 12:12:19 AM. This article is licensed under a Creative Commons Attribution-NonCommercial 3.0 Unported Licence.

measurement. As shown in Fig. 3a, distinct crystallization peaks (12°–27°) were observed for P1, P2, P3 and P4. The good crystallization could also be proved by the high melting point (286 °C) and crystallization temperature (247 °C) of P3 (Fig. 3f). Fortunately, from the high-resolution TEM (HRTEM) images of these linear polymers (Fig. S6–S9†), we captured an interplanar spacing of 0.43 nm for P1, 0.56 nm for P2, 0.42 nm for P3, 0.39 nm for P4, which are in good agreement with the corresponding XRD patterns from the Bragg formula. The molecular weight of the obtained polymer could be measured by GPC. The molecular weight is about 1.0×10^4 Da for P2 (Fig. 3g), suggesting that one polymer chain of P2 contained about 96 monomeric units. Furthermore, N_2 adsorption and desorption isotherms at 77 K suggest that all polymers have porous structures due to the bending and stacking of flexible polymer chains. Both P1 and P2 are quasi-type H_3 adsorption curves, indicating that they have lamellar structures. As for P3 and P4, quasi-type I adsorption curves are presented, indicating that both of them have microporous structures, and the microporous absorption is gradually increased from 3.5 to 10.3 $cm^3\ g^{-1}$ at a low relative pressure of P/P_0 ($\leq$0.001). Calculated from the isotherms, the Brunauer–Emmett–Teller surface area (S_{BET}) of polymers changed from 92 $m^2\ g^{-1}$ (P1), 180 $m^2\ g^{-1}$ (P2), and 64 $m^2\ g^{-1}$ (P3) to 93 $m^2\ g^{-1}$ (P4) (Fig. 3b–e). Pore size distributions calculated by the quenched-solid density functional theory (QSDFT) method demonstrate the transition of polymer structures from mesoporous (P1 and P2) to microporous (P3 and P4). Therefore, the resultant novel linear polymers of P1–P4 were endowed with good crystallinity, high melting points, good thermostability and porosity.

The successful C(sp^3)–C(sp^3) coupling polymerizations of dibromomethyl arenes motivate us to explore the Ni$(COD)_2$-catalyzed polymerizations of tri-/tetra-bromomethyl arenes, such as 1,3,5-tri-bromomethyl benzene, 1,2,4,6-tetra-bromomethyl benzene and tetrakis(4-(bromomethyl) phenyl)methane. Compared with HCPs synthesized by Friedel–Crafts reactions of arenes with dihaloalkanes, these polymerizations could produce three-dimensional flexible porous polymers with well-defined structures through precise C(sp^3)–C(sp^3) coupling that might show great advantages in gas adsorption and separation. Moreover, these porous polymers may possess higher porosity and greater spatial extensibility than the linear polymers because of the more alkane reaction sites (C–Br) in these monomers. Meanwhile, for the monomers of tri-/tetra-bromomethyl arenes, the large rotation freedom of saturated alkanes and benzene rings can endow the porous polymers with good structural flexibility (see experimental procedures in the ESI†). As illustrated in Fig. 4, three novel PAFs (PAF-64, PAF-65 and PAF-66) have been achieved with high conversion by using the Ni$(COD)_2$ catalytic system. The FTIR spectra of these PAFs have been obtained as shown in Fig. S14.† The bands associated with C–Br vibrations at 586 cm^{-1}, 603 cm^{-1}, and 621 cm^{-1} in the monomers were no longer present in PAF-64, PAF-65 and PAF-66, respectively, and the stretching vibration of C–H bonds of alkanes at ~2980 cm^{-1} was obviously strengthened in these PAFs. These results primarily indicated that the C(sp^3)–C(sp^3) cross-coupling polymerizations have successfully occurred.

The chemical structures of PAF-64, PAF-65 and PAF-66 were further characterized using the solid-state ^{13}C NMR spectra, as shown in Fig. 4b–d. Taking PAF-66 as an example, the intense signals at approximately δ = 146, 139 and 128 ppm can be assigned to the carbon atoms of the benzene ring, while the relatively weak signal at δ = 65 ppm can be assigned to the quaternary carbon atom that is connected to four phenyl groups and the signal at δ = 38 ppm is attributed to the alkyl carbon (Fig. 4d). The pore structures of the three porous polymers were investigated by physical nitrogen sorption. Their adsorption and desorption isotherms are shown in Fig. 4e–g, which are typical quasi-type I adsorption curves. The uptakes in the three isotherms increase gradually at low relative pressures of P/P_0 ($\leq$0.01), indicating that the microporous structures are gradually increasing. Increasing Brunauer–Emmett–Teller surface areas (S_{BET}) are achieved: 147 $m^2\ g^{-1}$, 347 $m^2\ g^{-1}$ and 390 $m^2\ g^{-1}$ for PAF-64, PAF-65 and PAF-66, respectively. To the best of our knowledge, PAF-66 possesses much higher specific surface area than the previous analogues (37 $m^2\ g^{-1}$ and 2.5 $m^2\ g^{-1}$) prepared by the reaction of tetraphenylmethane with dichloromethane/1,2-dichloroethane.[25,26] The pore size distributions were calculated using the quenched-solid density functional theory (QSDFT) method. PAF-64 has a mesoporous structure (2.8 nm, 4.6 nm, 7.1 nm), and PAF-65 has a microporous–mesoporous structure (1.7 nm, 3.9 nm, 4.0 nm). PAF-66 has mainly a microporous structure (1.23 nm). This might be because more reaction sites effectively occupy pore space, causing a smaller pore in the polymer. On the other hand, with the increase in freedoms or flexibility in monomers, the polymerization process can move towards the energy optimal direction, and finally a more regular pore structure and higher surface areas can be obtained. Besides, no distinct diffraction peaks were detected except for a broad peak for PAF-64 and PAF-65 by powder X-ray diffraction (PXRD) measurement (Fig. S15†), indicating their amorphous structures. Interestingly, another broad peak at 7°–11.2° for PAF-66 was observed and corresponded to 0.79–1.26 nm from the Bragg formula, which is in agreement with a pore size of 1.23 nm. SEM and TEM images show that the three PAFs are composed of spherical particles with 10–100 nm diameters (Fig. S16†). Thermogravimetric analysis shows that the synthesized polymers exhibit excellent thermal stability, $T_{d,10\%\ loss}$ > 442 °C (Fig. S17†). In addition, it was found that these PAFs have good resistance to acids and alkalis detected by infrared spectroscopy (Fig. S18†). The excellent structure features of these flexible PAFs inspire us to explore them for high pressure methane storage.

ANG technology is a viable alternative to traditional liquefied or compressed natural-gas storage. It's worth noting that working capacity (deliverable capacity) is crucial instead of total adsorption capacity in the performance evaluation of adsorbents for ANG storage systems. Working capacity is defined as the amount of gas released from the maximum adsorption pressure (*i.e.*, 100 bar) to the minimum desorption pressure (generally, 5 bar). Obviously, the working capacity is less than the storage capacity.[25] Methane adsorption for the three flexible porous polymers (PAF-64, PAF-65 and PAF-66) was measured at 273 K and 288 K using a next generation gravimetric sorption

Open Access Article. Published on 07 June 2024. Downloaded on 2/25/2026 12:12:19 AM.
This article is licensed under a Creative Commons Attribution-NonCommercial 3.0 Unported Licence.

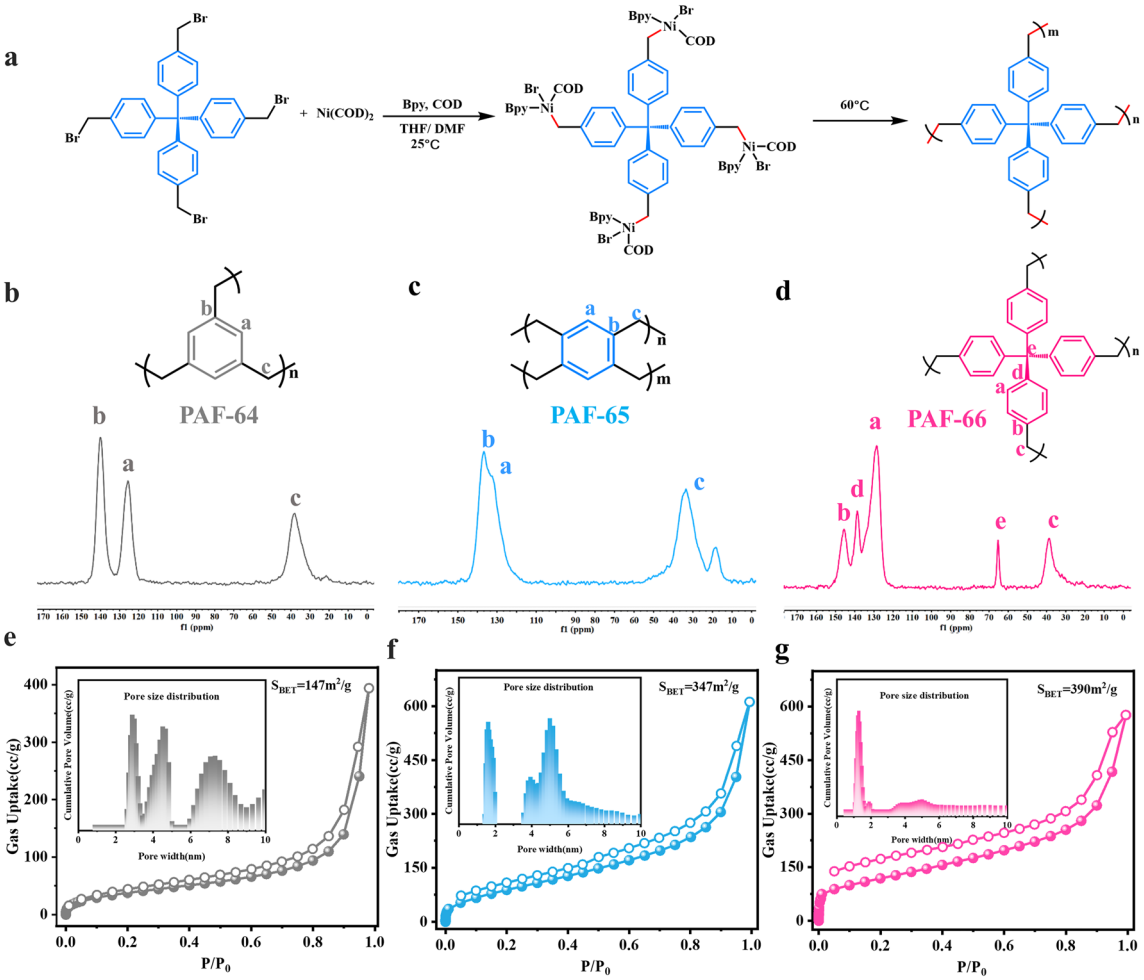

Fig. 4 Synthesis and characterization of flexible porous polymers. (a) The synthetic pathway to produce the porous polymers. Solid-state ^{13}C NMR spectra of PAF-64 (b), PAF-65 (c) and PAF-66 (d). N_2 adsorption–desorption isotherms measured at 77 K and the corresponding pore size distributions for PAF-64 (e), PAF-65 (f) and PAF-66 (g).

analyzer (XEMIS). We also explored the relationship between surface areas/flexibility and CH_4 uptake. The results showed that all polymers displayed a considerable adsorption capacity for CH_4 at 273 K and a lower CH_4 uptake due to the exothermic process at 288 K. To further investigate the gas–matrix interaction, CH_4 adsorption enthalpy (-14.7 kJ mol^{-1}) of PAF-66 was obtained (Fig. S19†), which was in line with the simulated result (Fig. S24a†). As illustrated in Fig. 5a, b and S20,† methane absorption increased evenly to 100 bar for all PAFs without reaching saturation, and they showed the characteristics of flexible porous polymers.[26] Since the adsorption processes are carried out under constant temperature conditions, any change in finite charge (chemical adsorption) or in the pore structure (gate-opening behaviour) will cause a sudden change in the adsorption curve. Thus, for the PAFs, increasing pressure extends the space volume of flexible polymers, and they showed a pressure-triggered structure (swelling behavior), which was further confirmed using the theoretical calculations (Fig. S25†). Furthermore, these PAFs also showed a swelling behavior when placed in organic solvent (THF) as shown in Fig. S21.† The volume expands 2–3 times compared with the original. Their adsorption capacities range from 6.8 g g^{-1}(PAF-64) and 8.3 g g^{-1} (PAF-65) to 9.8 g g^{-1} (PAF-66) depending on different flexibilities. Thus, PAF-66 has the highest adsorption capacity among the three PAFs and this further confirms that the adsorption capacity is mainly determined using flexibility.

Flexible PAF-64, PAF-65 and PAF-66 show an outstanding gravimetric working capacity (5–100 bar) of 0.32 g g^{-1}, 0.38 g g^{-1} and 0.46 g g^{-1}, respectively at 273 K. PAF-66 possesses the highest CH_4 uptake owing to its more flexible sites compared to PAF-64 and PAF-65. Meanwhile, PAF-66 is comparable with other previously reported adsorbents for ANG technology (Fig. 5d).[17,18,24–26,31–34] Interestingly, we found that the CH_4 uptake of these PAFs is consistent with the specific surface area and flexibility. Based on bulk tap density of PAF-64 (0.46 g cm^{-3}), PAF-65 (0.47 g cm^{-3}) and PAF-66 (0.50 g cm^{-3}) (Fig. S22†), all PAFs showed a high volumetric working capacity (5–100 bar) of 206 cm^3 cm^{-3}, 255 cm^3 cm^{-3} and 313 cm^3 cm^{-3}, respectively. This flexible PAF-66 is comparable with other best-performing adsorbents, such as COP-150 (294 cm^3 cm^{-3}, 273 K, 100 bar),[24] NU-111 (267 cm^3 cm^{-3}, 240 K, 65 bar)[29] and Co(bdp) (220 cm^3 cm^{-3}, 273 K, 65 bar).[18] To our knowledge, PAF-66 (313

© 2024 The Author(s). Published by the Royal Society of Chemistry

Open Access Article. Published on 07 June 2024. Downloaded on 2/25/2026 12:12:19 AM.
This article is licensed under a Creative Commons Attribution-NonCommercial 3.0 Unported Licence.

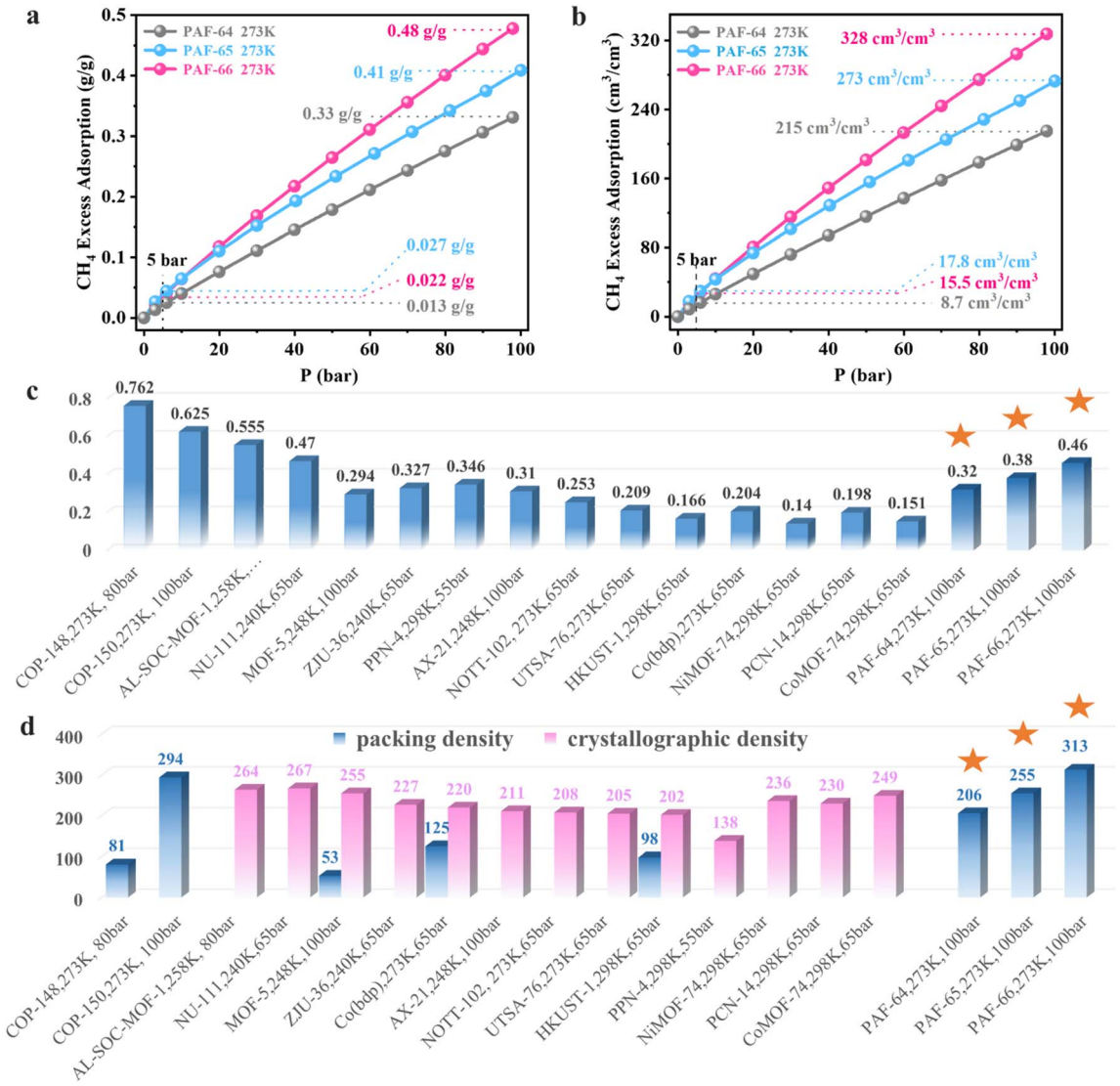

Fig. 5 Gravimetric methane adsorption isotherms (a) and volumetric methane adsorption (b) of PAF-64, PAF-65 and PAF-66 at 273 K. (c) Comparison of gravimetric methane working capacities with those of some adsorbents. (d) Comparison of volumetric methane working capacities with those of some adsorbents.

cm^3 cm^{-3}) shows the highest value of volumetric working capacity among the reported porous materials, 19% above the US DOE target (263 cm^3 cm^{-3}) (Fig. 5e). Undoubtedly, these flexible PAFs generated by $C(sp^3)$–$C(sp^3)$ coupling polymerization show flexible adsorptive behavior and are excellent ANG materials owing to their high methane-adsorption and outstanding structural stability.

Conclusions

In summary, we have developed novel and highly efficient $C(sp^3)$–$C(sp^3)$ coupling reactions by using $Ni(COD)_2$ systems and produced linear crystalline polymers and flexible PAFs with well-defined structures. The linear crystalline polymers with high melting points and moderate porosity can be regarded as alternating copolymers of ethylene and benzene, which are hardly obtained by traditional polymerization methods. Moreover, the flexible PAFs stemmed from tri-/tetra-bromomethyl arenes show high surface area and excellent acid/alkali stability and thermostability. Remarkably, these PAFs exhibit high methane-storage capacity because of their flexible frameworks. Especially for PAF-66, the highest volumetric working capacity of 313 cm^3 cm^{-3} for methane was achieved, which is much higher than the US DOE target. It is indisputable that the flexible PAFs are viable adsorbents for natural gas. This study opens up a new avenue for the construction of porous polymers by high efficient $C(sp^3)$–$C(sp^3)$ coupling and provides a feasible strategy for the design of high-capacity methane storage materials.

Data availability

All relevant data are available from the corresponding authors upon reasonable request.

Open Access Article. Published on 07 June 2024. Downloaded on 2/25/2026 12:12:19 AM. This article is licensed under a Creative Commons Attribution-NonCommercial 3.0 Unported Licence.

Author contributions

D. Liu and G. Zhu conceived and designed the experiments. S. Zhou performed experiments and data analysis. T. Qiu assisted with the mechanism of methane adsorption. H. Wang and B. Tang assisted with the materials synthesis and characterization. Y. Su, T. Nan, J. Dong, and Z. Wang contributed to the discussion. D. Liu, S. Zhou and G. Zhu wrote the manuscript together.

Conflicts of interest

There are no conflicts to declare.

Acknowledgements

This work was partially supported by the National Natural Science Foundation of China (No. 22071021, 22131004, and U21A20330) and the "111" project (No. B18012).

Notes and references

1 Q. Hao, Y. Tao, X. Ding, Y. Yang, J. Feng, R.-L. Wang, X.-M. Chen, G.-L. Chen, X. Li, H. OuYang, X. Hu, J. Tian, B.-H. Han, G. Zhu, W. Wang, F. Zhang, B. Tan, Z.-T. Li, D. Wang and L.-J. Wan, Porous Organic Polymers: a Progress Report in China, *Sci. China: Chem.*, 2023, **66**, 620–682.

2 T. Ben, H. Ren, S. Ma, D. Cao, J. Lan, X. Jing, W. Wang, J. Xu, F. Deng, J. M. Simmons, S. Qiu and G. Zhu, Targeted Synthesis of a Porous Aromatic Framework with High Stability and Exceptionally High Surface Area, *Angew. Chem., Int. Ed.*, 2009, **48**, 9457–9460.

3 W. Lu, D. Yuan, D. Zhao, C. I. Schilling, O. Plietzsch, T. Muller, S. Brase, J. Guenther, J. Blumel, R. Krishna, Z. Li and H. Zhou, Porous Polymer Networks: Synthesis, Porosity, and Applications in Gas Storage/Separation, *Chem. Mater.*, 2010, **22**, 5964–5972.

4 R. Dawson, A. Laybourn, Y. Z. Khimyak, D. J. Adams and A. I. Cooper, High Surface Area Conjugated Microporous Polymers: The Importance of Reaction Solvent Choice, *Macromolecules*, 2010, **43**, 8524–8530.

5 H. Ma, H. Ren, X. Zou, S. Meng, F. Sun and G. Zhu, Post-metalation of Porous Aromatic Frameworks for Highly Efficient Carbon Capture from CO_2 + N_2 and CH_4 + N_2 Mixtures, *Polym. Chem.*, 2014, **5**, 144–152.

6 S. Zhou, Z. Liu, P. Zhang, H. Rong, T. Ma, F. Cui, D. Liu, X. Zou and G. Zhu, Tailoring the Pore Chemistry in Porous Aromatic Frameworks for Selective Separation of Acetylene from Ethylene, *Chem. Sci.*, 2022, **13**, 11126–11131.

7 C. P. Johnston, R. T. Smith, S. Allmendinger and D. W. C. MacMillan, Metallaphotoredox-Catalyzed sp^3–sp^3 Cross-Coupling of Carboxylic Acids with Alkyl Halides, *Nature*, 2016, **536**, 322–325.

8 S. Wang, C. Zhang, Y. Shu, S. Jiang, Q. Xia, L. Chen, S. Jin, I. Hussain, A. I. Cooper and B. Tan, Layered Microporous Polymers by Solvent Knitting Method, *Sci. Adv.*, 2017, **3**, e1602610.

9 C. E. I. Knappke, S. Grupe, D. Grtner, M. Corpet, C. Gosmini and A. J. Wangelin, Reductive Cross-Coupling Reactions between Two Electrophiles, *Chem.–Eur. J.*, 2014, **20**, 6828–6842.

10 Y. Cai, X. Qian and C. Gosmini, Cobalt-Catalyzed C_{sp3}–C_{sp3} Homocoupling, *Adv. Synth. Catal.*, 2016, **358**, 2427–2430.

11 Y. Liu, S. Xiao, Y. Qi and F. Du, Reductive Homocoupling of Organohalides Using Nickel(II) Chloride and Samarium Metal, *Chem.–Asian J.*, 2017, **12**, 673–678.

12 O. Vogl, M. F. Qin and A. Zilkha, Head to Head Polymers, *Prog. Polym. Sci.*, 1999, **24**, 1481–1525.

13 L. Zou, M. Long, H. Zhou, W. Zhu, K. Zhang, Y. Chen and F. Xi, $C(sp^3)$–$C(sp^3)$ Coupling Polymerization of Alkyl Dibromides for Preparation of Polymers with Precisely Located Phenyl Pendants, *Polymer*, 2015, **64**, 196–201.

14 Z. Wang, J. Duan, S. Chen, Y. Fu, X. Li, D. Wang, M. Zhang, Z. Zhang, D. Liu and F. Wang, A Review on High-Density Methane Storage in Confined Nanospace by Adsorption-Hydration Hybrid Technology, *Chem.–Eur. J.*, 2022, **50**, 104195.

15 E. I. Knerelman, Y. A. Karozina, I. G. Shunina and I. V. Sedov, Highly Porous Materials as Potential Components of Natural Gas Storage Systems: Part 2 (A Review), *Pet. Chem.*, 2022, **62**, 677–713.

16 Y. Peng, V. Krungleviciute, I. Eryazici, J. T. Hupp, O. K. Farha and T. Yildirim, Methane Storage in Metal–Organic Frameworks: Current Records, Surprise Findings, and Challenges, *J. Am. Chem. Soc.*, 2013, **135**, 11887–11894.

17 J. A. Mason, M. Veenstra and J. R. Long, Evaluating Metal–Organic Frameworks for Natural Gas Storage, *Chem. Sci.*, 2014, **5**, 32–51.

18 J. A. Mason, J. Oktawiec, M. K. Taylor, M. R. Hudson, J. Rodriguez, J. E. Bachman, M. I. Gonzalez, A. Cervellino, A. Guagliardi, C. M. Brown, P. L. Llewellyn, N. Masciocchi and J. R. Long, Methane Storage in Flexible Metal–Organic Frameworks with Intrinsic Thermal Management, *Nature*, 2015, **527**, 357–361.

19 Y. Lin, C. Kong, Q. Zhang and L. Chen, Metal–Organic Frameworks for Carbon Dioxide Capture and Methane Storage, *Adv. Energy Mater.*, 2017, **7**, 1601296.

20 Z. Chen, P. Li, R. Anderson, X. Wang, X. Zhang, L. Robison, L. R. Redfern, S. Moribe, T. Islamoglu, D. A. Gómez-Gualdrón, T. Yildirim, J. F. Stoddart and O. K. Farha, Balancing Volumetric and Gravimetric Uptake in Highly Porous Materials for Clean Energy, *Science*, 2020, **368**, 297–303.

21 B. C. D. Wood, B. Tan, A. Trewin, F. Su, M. J. Rosseinsky, D. Bradshaw, Y. Sun, L. Zhou and A. I. Cooper, Microporous Organic Polymers for Methane Storage, *Adv. Mater.*, 2008, **20**, 1916–1921.

22 S. Bracco, D. Piga, I. Bassanetti, J. Perego, A. Comotti and P. Sozzani, Porous 3D polymers for high pressure methane storage and carbon dioxide capture, *J. Mater. Chem. A*, 2017, **5**, 10328–10337.

23 Y. He, W. Zhou, G. Qian and B. Chen, Methane Storage in Metal–Organic Frameworks, *Chem. Soc. Rev.*, 2014, **43**, 5657–5678.

© 2024 The Author(s). Published by the Royal Society of Chemistry

Open Access Article. Published on 07 June 2024. Downloaded on 2/25/2026 12:12:19 AM.
This article is licensed under a Creative Commons Attribution-NonCommercial 3.0 Unported Licence.

24 G.-Q. Kong, Z.-D. Han, Y. He, S. Ou, W. Zhou, T. Yildirim, R. Krishna, C. Zou, B. Chen and C.-D. Wu, Expanded Organic Building Units for the Construction of Highly Porous Metal–Organic Frameworks, *Chem.–Eur. J.*, 2013, **19**, 14886–14894.

25 S. Yang, X. Wang and B. Tan, Porosity Engineering of Hyper-Cross-Linked Polymers Based on Fine-Tuned Rigidity in Building Blocks and High-Pressure Methane Storage Applications, *Macromolecules*, 2023, **56**, 1213–1222.

26 V. Rozyyev, D. Thirion, R. Ullah, J. Lee, M. Jung, H. Oh, M. Atilhan and C. T. Yavuz, High-Capacity Methane Storage in Flexible Alkane-Linked Porous Aromatic Network Polymers, *Nat. Energy*, 2019, **4**, 604–611.

27 C. F. Martın, E. Stockel, R. Clowes, D. J. Adams, A. I. Cooper, J. J. Pis, F. Rubieraa and C. Pevida, Hypercrosslinked Organic Polymer Networks as Potential Adsorbents for Pre-combustion CO_2 Capture, *J. Mater. Chem.*, 2011, **21**, 5475.

28 S. Grätz, S. Zink, H. Kraffczyk, M. Rose and L. Borchardt, Mechanochemical Synthesis of Hyper-Crosslinked Polymers: Influences on Their Pore Structure and Adsorption Behaviour for Organic Vapors, *Beilstein J. Org. Chem.*, 2019, **15**, 1154–1161.

29 W. Shi, C. Liu and A. Lei, Transition-metal catalyzed oxidative cross-coupling reactions to form C–C bonds involving organometallic reagents as nucleophiles, *Chem. Soc. Rev.*, 2011, **40**, 2761–2776.

30 T. Mamaoto, S. Wakabayashi and K. Osakada, Mechanism of C–C coupling reactions of aromatic halides, promoted by $Ni(COD)_2$, in the presence of 2,2′-bipyridine and PPh_3, to give biaryls, *J. Organomet. Chem.*, 1992, **428**, 223–237.

31 D. Alezi, Y. Belmabkhout, M. Suyetin, P. M. Bhatt, Ł. J. Weselinski, V. Solovyeva, K. Adil, I. Spanopoulos, P. N. Trikalitis, A.-H. Emwas and M. Eddaoudi, MOF Crystal Chemistry Paving the Way to Gas Storage Needs: Aluminum-Based soc-MOF for CH_4, O_2, and CO_2 Storage, *J. Am. Chem. Soc.*, 2015, **137**, 13308–13318.

32 Y. He, W. Zhou, T. Yildirim and B. Chen, A Series of Metal–Organic Frameworks with High Methane Uptake and An Empirical Equation for Predicting Methane Storage Capacity, *Energy Environ. Sci.*, 2013, **6**, 2735–2744.

33 D. Yuan, W. Lu, D. Zhao and H. Zhou, Highly Stable Porous Polymer Networks with Exceptionally High Gas-Uptake Capacities, *Adv. Mater.*, 2011, **23**, 3723–3725.

34 J. Jiang, H. Furukawa, Y.-B. Zhang and O. M. Yaghi, High Methane Storage Working Capacity in Metal-Organic Frameworks with Acrylate Links, *J. Am. Chem. Soc.*, 2016, **138**, 10244–10251.